optica

Brightness enhancement in a solid-state laser by mode transformation

DARRYL NAIDOO,[1,2,*] (ID) IGOR A. LITVIN,[1] AND ANDREW FORBES[2] (ID)

[1]CSIR National Laser Centre, P.O. Box 395, Pretoria 0001, South Africa
[2]School of Physics, University of the Witwatersrand, Private Bag 3, Wits 2050, South Africa
*Corresponding author: dnaidoo3@csir.co.za

Laser brightness is a measure of the ability to deliver intense light to a target and encapsulates both the energy content and the beam quality. High-brightness lasers require that both parameters be maximized, yet standard laser cavities do not allow this. For example, multimode beams, a mix of many transverse modes, have a high energy content but low beam quality, while single transverse mode Gaussian beams have a good beam quality, but their small mode volume means a low energy extraction. Here we overcome this fundamental limitation and demonstrate an optimal approach to realizing high-brightness lasers. We employ intra-cavity beam shaping to produce a single transverse mode that changes profile inside the cavity, Gaussian at the output end and flattop at the gain end, such that both energy extraction and beam quality are simultaneously optimized. This work should have a significant influence on the design of future high-brightness laser cavities.   © 2018 Optical Society of America under the terms of the OSA Open Access Publishing Agreement

OCIS codes: (140.3300) Laser beam shaping; (140.3580) Lasers, solid-state; (060.5060) Phase modulation.

https://doi.org/10.1364/OPTICA.5.000836

1. INTRODUCTION

The brightness of a laser source is a characteristic that encapsulates the energy or power content and the quality of the laser mode, requiring both to be optimized, i.e., maximal energy in a good beam quality. Bright sources are of particular importance in applications where high energy is to be delivered to some distant target, in laser materials processing where high power is required at some specific plane, and in long distance free-space optical communication. The brightness, B, describes the potential of a laser beam to achieve high intensities while maintaining a large Rayleigh range for small focusing angles, which is strongly dependent on the quality of the transverse mode at the output and is defined as the power (P) emitted per unit surface area (A) per unit solid angle (Ω). This can be expressed in terms of the beam quality factor, M^2, as

$$B = \frac{P}{A\Omega} = \frac{P}{(M^2)^2\lambda^2}, \qquad (1)$$

where $M^2 = 4\pi\sigma\sigma_s/\lambda = \pi w_0\theta_0/\lambda$, and σ represents the second-moment real beam variance corresponding to the time-averaged intensity profile, while σ_s corresponds to the spatial frequency distribution, and λ represents the wavelength of the laser beam [1]. We have also expressed this in terms of the beam waist and half-angle divergence, w_0 and θ_0, respectively, so that the laser beam may be expressed as $A = \pi w_0^2 = 4\pi\sigma^2$, and the solid angle is expressed as $\Omega = \pi\theta_0^2 = 4\pi\sigma_s^2$. Brightness is therefore proportional

to the beam's power (energy) and is inversely proportional to the quality of the mode.

There have been many extra-cavity approaches to improving brightness from laser sources, from the use of fiber lasers [2,3], to coherent beam combining [4–6], to semiconductor lasers [7–9]. Intra-cavity approaches, however, have seen much interest over a number of years [10–12] and are highly attractive for improving laser brightness, as they potentially offer better pump-to-mode overlap, thus enabling higher energy extraction with an improved beam quality at the output. There are several design configurations available that consider either low or higher order mode selection [13–19], and particular to the selection of flattop beams (FTBs) for increased energy extraction and single-mode operation, there are several phase-only approaches that include the use of diffractive mirrors [20], graded-phase mirrors [21,22], diffractive elements [23], and intra-cavity deformable mirrors [24–29]. Other approaches include an intra-cavity amplitude filter [30], manipulation of the gain profile [31], an intra-cavity variable reflectivity mirror [32], and employing optical feedback in a microchip laser [33]. With many of these approaches, an obvious step in realizing high brightness in solid-state lasers is through increasing the output laser power by scaling up the input pump power. Doing this is known to increase the thermal load in the laser material, giving rise to a nonuniform temperature distribution. In the case of solid-state lasers, this results in the generation of phase aberrations, which perturb the oscillating mode so that the beam quality degrades. In the worst cases, the increase in

power is negated by the decrease in beam quality so that the net result is a brightness that does not change or, worse, actually decreases. For this reason, it is understood that increasing the input pump power is limited in achieving high-brightness lasers [12,34–37]. Alternatively, one may maximize the beam quality factor through exciting a low-order mode, but this is usually at the expense of energy extraction due to a smaller gain volume. Thus, conventional solid-state laser paradigms dictate that it is not possible to simultaneously maximize both the mode quality and mode energy, and thus brightness cannot be optimized.

In this paper, we show how a laser cavity can be designed to maximize the mode extraction volume and the mode quality simultaneously, thus optimizing the brightness. Using a diode-pumped solid-state laser as an example, we employ intra-cavity beam-shaping optics to force what we call "mode metamorphosis": our laser is designed to have an FTB at the gain end of the cavity and a Gaussian beam at the output coupler (OC) end. This approach breaks the standard design paradigm that a mode of a cavity is a particular beam (e.g., Gaussian or flattop) everywhere, i.e., for a Gaussian beam to exit a cavity, it is assumed that the cavity mode is Gaussian everywhere. Here, the beam at any given position repeats after every round trip but changes everywhere along the length of the cavity, from one intensity profile to another. It is this freedom to engineer the cavity mode at different locations that allows brightness to be optimized. For example, the consequence of ensuring an FTB at the gain end is that the entire gain volume is used, thus maximizing energy extraction while delivering this energy in a low-divergence Gaussian beam at the output end of the cavity. We apply our approach to an otherwise standard cavity and demonstrate a 350% increase in brightness, which with some optimization could be doubled. Finally, we point out the general nature of this approach and how it may be applied to other cavity geometries.

2. CONCEPT AND SIMULATIONS

In what follows, we will use the notation of modes to represent the transverse modes of the cavity. Note that we use the correct terminology, where TEM_{00} refers to the lowest loss mode of the cavity, TEM_{01} the next lowest loss, and so on, and do not specify a family of modes, e.g., Gaussian, Hermite–Gaussian or Laguerre–Gaussian, and so on.

Our idea is based on the ability to create a cavity that supports a single transverse mode, TEM_{00}, that does not have the same intensity profile everywhere in the cavity yet repeats at each position after one round trip. In particular, we wish to create a cavity with a TEM_{00} mode that has a Gaussian intensity profile at the OC end and a flattop intensity profile at the other. This is a well-known beam-shaping problem both inside and outside the laser cavity [13,14,16,17,20,21,38,39]. By employing a cavity with two beam-shaping elements, we are able to have a mode that changes continuously in shape during propagation from one mirror to the other, morphing from a Gaussian profile to a flattop profile, yet remains a single transverse mode of the cavity. This is a paradigm shift in how one thinks about cavity modes. We are familiar with the idea that the transverse modes can change size throughout the cavity; now we show that they can be made to change intensity profile too. An important aspect is that we use two phase-only elements for the transformation; this allows the beam shaping to be done in a lossless manner, thus minimizing cavity losses.
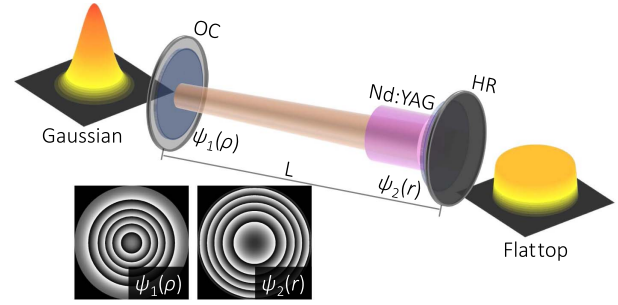
Fig. 1. Schematic showing the metamorphosis of a Gaussian beam into an FTB with two phase-only optical elements. The first optical element, $\psi_1(\rho)$, is used to transform a Gaussian field into a flattop. The second element, $\psi_2(r)$, is encoded as the conjugate of the field at that plane such that the output FTB has a flat wavefront. Both elements have a phase variation of 0–2π (white to black) and are depicted as gray-scale images.

To design our two phase-only optics, we consider the desired beam at the OC as in Fig. 1 to be a Gaussian field with a flat wavefront of the form

$$u_G(\rho) = \exp\left[-\left(\frac{\rho}{w_0}\right)^2\right],$$

where w_0 is the Gaussian beam width (at the OC). We wish to transform this into an FTB at the gain end, with a constant intensity profile in some well-defined region, and zero elsewhere [16,39]:

$$u_{\text{FTB}}(\rho) = \begin{cases} 1 & \text{for } |\rho| < w_{\text{FTB}}, \\ 0 & \text{for } |\rho| > w_{\text{FTB}}, \end{cases}$$

where w_{FTB} is the width of the flattop. We note that although the design calls for this ideal profile, the spatial frequency spectrum requires infinitely large apertures, and thus in practice, only approximations to it are expected. If the element at the OC comprises a Fourier transforming lens and some phase-only transmission component, ψ_F, and if the optical length of the cavity matches that of the Fourier transforming lens ($L = f$), then we may determine an analytical solution for the phase function of the first element through the stationary phase approximation [16,17,39]:

$$\psi_1(\rho) = \psi_F(\rho) - \frac{k\rho^2}{2f}, \tag{2}$$

where the term $k\rho^2/2f$ is required for the lens and

$$\psi_F(\rho) = \alpha \frac{\sqrt{\pi}}{2} \int_0^{\rho/w_0} \sqrt{1 - \exp(-\xi^2)}\,\mathrm{d}\xi, \tag{3}$$

where α is a dimensionless parameter that is defined as

$$\alpha = \frac{2\pi w_0 w_{\text{FTB}}}{f\lambda}. \tag{4}$$

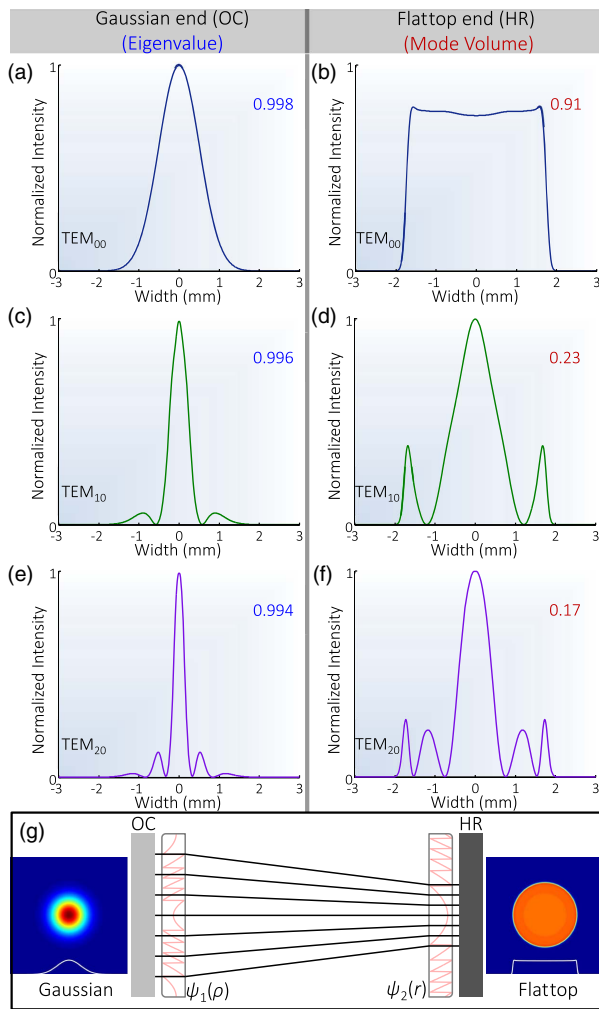As with the phase profile of the first element, ψ_1, it is also possible to apply the stationary phase approximation to determine a closed-form solution for the phase profile of the second element at the planohigh-reflecting (HR) mirror as

$$\psi_2(r) = \arg\left\{ \exp\left[i\left(\frac{kr^2}{2f} + \psi_F(\vartheta(r)) - \frac{\alpha r \vartheta(r)}{w_0 w_{\text{FTB}}} \right) \right] \right\}, \tag{5}$$

where the unknown function $\vartheta(r)$ may be determined from the stationary phase condition $r/w_{\text{FTB}} = \partial\psi_F/\partial\rho$. This ensures that

the flattop output has a flat wavefront that when reverse propagated, due to the reciprocity of light, morphs into a Gaussian beam at the OC.

In order to test the concept, we performed a matrix-style Fox–Li simulation [16] of the empty cavity (cavity without gain) to determine whether the fundamental TEM_{00} mode is as desired and to determine the competing modes. By starting the simulation with random noise and running until convergence, the resulting eigenvectors return the mode type and the eigenvalues that are the losses associated with the mode. The results of this simulation at both the OC and gain end of the cavity are shown in Fig. 2. We note that indeed the lowest loss mode of the cavity is a structure that morphs from a Gaussian profile to a flattop, as seen in Figs. 2(a) and 2(b), while the next two competing modes (TEM_{10} and TEM_{20}) likewise morph in profile but are not the

desired profiles. Contrary to usual cavity dynamics, here the eigenvalues associated with each mode (shown in blue) are very similar, implying poor mode discrimination by diffraction losses alone.
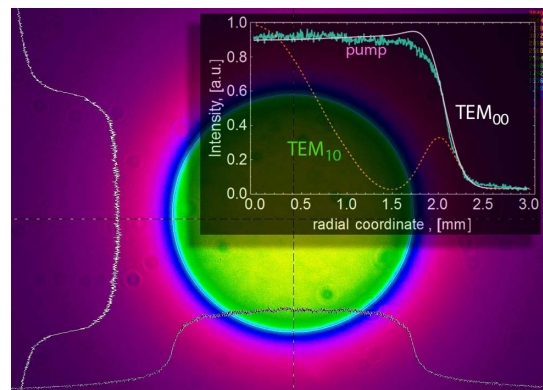
Without any other considerations, such a cavity would lase on several of these transverse modes. But an important aspect of our concept is that the intensity profile of the mode at the gain end should match as closely as possible to the gain profile. It is known that the overlap between the mode and the gain has a significant influence on the mode competition [40], since gain is the complement to loss inside lasers; that is to say, as the cavity lases when gain equals loss, increasing one is tantamount to decreasing the other.

This overlap can be described by

$$\eta = \frac{\langle \text{TEM}_{nm}|M_p\rangle}{\langle \text{TEM}_{nm}|\text{TEM}_{nm}\rangle\langle M_p|M_p\rangle}, \tag{6}$$

where M_p is the pump mode and the braces represent the usual inner product of two fields.

Here the overlap efficiency for the TEM_{00} mode is 91%, the TEM_{10} mode is 23%, and the TEM_{20} mode is 17%, shown as red text in Fig. 2. This demonstrates that the TEM_{00} mode has a better pump-to-mode overlap and thus preferential gain as compared to the next lowest loss mode. This can be used to discriminate the modes. We design the intensity profile of the desired mode at the gain end to match the fluorescence of the gain to be used in our experiments (illustrated in Fig. 3 for our example). Although the diffraction losses for the first three competing modes is less than 1%, the diffraction losses are insignificant in the selection of the output mode; however, the pump-to-mode overlap of the fundamental mode provides the required modal discrimination. This is supported by our design, which predicts convergence to the desired mode with good discrimination. The convergence of the design also illustrates the stability of the cavity particular to the oscillation of the TEM_{00} mode. To illustrate the stability in our cavity, consider our starting plane to be represented by parallel rays corresponding to a collimated Gaussian beam, as in Fig. 2(g). Here the rays will be mapped by the first element to the plane of the second element, and since our

Fig. 2. We performed a matrix-style Fox–Li simulation of the cavity without gain and illustrate that the lowest loss mode is a structure that morphs from a (a) Gaussian profile at the OC to a (b) flattop at the HR. The next two competing modes at the (c) and (e) OC likewise morph in profile to the (d) and (f) HR but are far from the desired profiles. The resulting losses associated with the mode [(a), (c), (e) eigenvalues shown in blue] imply poor mode discrimination based on diffraction losses. The required discrimination is provided by gain-to-mode overlap with (b) 91% for the desired flattop, (d) 23% for TEM_{10} and (f) 17% for TEM_{20}. (g) Ray-tracing calculation showing that the ray trajectories are parallel at each mirror.

Fig. 3. Modal discrimination of higher unwanted modes is determined primarily by the pump-to-mode overlap and not by the modal diffraction losses. Here we show the fluorescence of the side-pumped gain medium used in our experiment, which closely approximates as flattop. The overlaps between this gain and the first two lowest loss modes in the cavity, TEM_{00} and TEM_{10}, respectively, are given by $\eta_{00} = 91\%$ and $\eta_{10} = 23\%$.

design approach to obtain the phase of the second element is through reverse propagation [13], the resulting output rays after the second element will also be parallel. This demonstrates that the rays will map back on themselves after every round trip, as the rays are parallel on both ends of the cavity. Furthermore, each element consists of a positive lensing component to aid stability in a conventional manner ($0 < g_1 g_2 < 1$). Although the cavity length is equivalent to the focal length of the lens embedded in the first element, the positive lensing component in the second element forces the cavity to be stable.

3. EXPERIMENTAL RESULTS

The concept of the laser resonator as presented in Fig. 1 was optically tested external to the laser cavity in an unfolded geometry, as illustrated in Fig. 4(a). The unfolded round trip simulates the propagation of the cavity mode from the OC to the HR and back along the same path. A single round trip requires four optical phase transformations, as we pass through each optical element twice. The intensity profiles immediately before and after each element are identical, although their phase compositions are markedly different. This implies that on the return intra-cavity pass (HR to OC), the intensity of the field immediately before $\psi_1(\rho)$ may be adequately analyzed to infer the intensity after the optical element.

We executed this experimentally using a spatial light modulator (SLM) (Holoeye, PLUTO-NIR, with 1080 pixels × 1920 pixels of 8 μm pitch and calibrated for a 2π phase shift) to mimic the phase transformation elements [see Fig. 4(b)]. We addressed the SLM with phase profiles, $\psi_1(\rho)$ and $2\psi_2(r)$, one to each half of the SLM, using a split-screen functionality. We directed a collimated Gaussian beam operating at $\lambda = 633$ nm with $w_0 = 1$ mm onto the left half of the SLM, as shown in Fig. 5(a). This half was addressed with a gray-scale phase pattern of the first element, which contained an encoded lens of $f = 250$ mm for the selection of an FTB of $2w_{FTB} = 3.6$ mm. The resulting reflected beam was propagated to a pop-up flat mirror (PFM) that was positioned at 125 mm from the SLM screen. With this mirror depressed, the output on CCD_1 (Spiricon Beamgage SP620U) resulted in a well-defined FTB at 250 mm from the plane of the SLM with a measured edge-to-edge diameter of 3.61 mm, as shown in Fig. 5(b). With the PFM acting in a

reflective capacity, the resulting beam was directed to the right half of the SLM screen, which was addressed with a gray-scale phase pattern of double the second element ($2\psi_2(r)$) to simulate a double pass. Since the PFM was positioned at 125 mm from the SLM screen, the resulting propagation distance between the left and right half of the screen was equivalent to the focal length of the encoded lens. Finally, the reflected beam off the right half of the SLM screen was propagated 250 mm and was captured on CCD_2 (Spiricon Beamgage SP620U) after reflection off a flat mirror (FM). The output field resulted in a Gaussian beam [see Fig. 5(c)] with a diameter of $4\sigma = 1.90$ mm (measured $w_0 = 0.95$ mm). This external test with SLMs served to confirm that the design principle works, and that while the cavity mode is always changing, it is nevertheless repeated after each round trip. The measured and calculated profiles were all in excellent agreement, both in terms of profile shape and size, as seen in Fig. 5. We do notice some noise overlaid with our desired profiles, which could be due to pixelation of the SLMs or the phase-wrapping of the phase functions. Such noise has high spatial frequency and would be expected to contribute to small additional losses inside the cavity.

The experimental implementation of the intra-cavity metamorphosis of a Gaussian beam to an FTB was realized in a diode-pumped solid-state laser where a 0.5 at. % Nd-doped YAG rod (4 mm × 50 mm) was side-pumped with a total input average pump power of ~600 W, where the input pump energy was pulsed at 20 pulses per second (20 pps), as illustrated in Fig. 6(a). The cavity mirrors were both planar ($R = \infty$), with the back mirror acting as a high reflector while the OC had a reflectivity of 40%. The optical elements were positioned sufficiently adjacent to the mirrors and were suitably mounted for accurate control of the lateral positioning and pitch and yaw. The length (L) of the cavity was adjusted to accommodate the gain medium and was increased from its nominal length of 538 mm (corresponding to the embedded lens of $f = 538$ mm) to 570 mm (see the values above the double-sided arrows in Fig. 6(a) indicating the position of each component in the cavity). To design optical elements based on this cavity, we opted for a Gaussian beam of $w_0 = 1.5$ mm with a transformation into an FTB of $w_{FTB} = 1.75$ mm. The elements were designed such that a flattop of 2 mm in diameter traversed the length of the crystal.
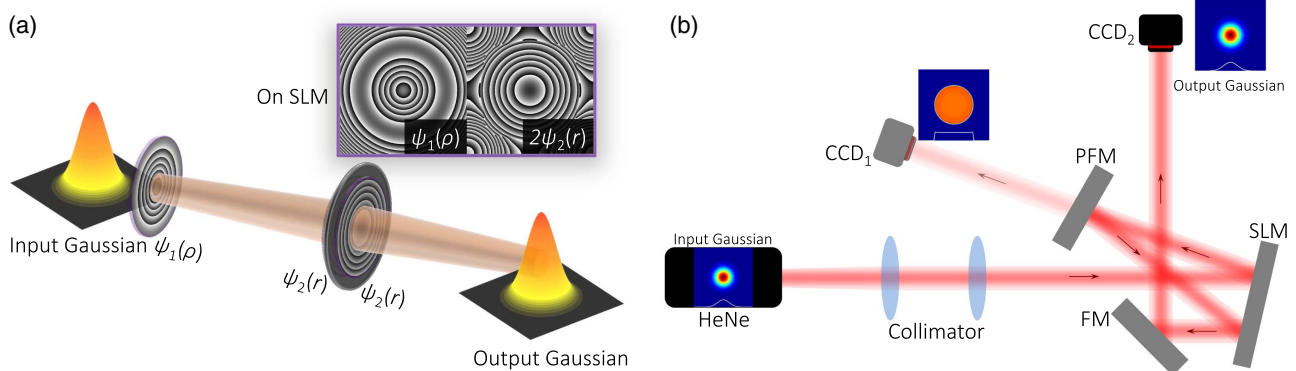
Fig. 4. (a) Single intra-cavity round trip may be represented as an unfolded cavity with two phase transformations. (b) The external optical testing of a single round trip was executed experimentally using a SLM using a split-screen functionality. The left half of the screen was addressed with a phase profile of the first element ($\psi_1(\rho)$), while the right half of the screen was addressed with a phase profile of double the second element ($2\psi_2(r)$). A collimated Gaussian beam was propagated to the left half of the screen, and the resulting flattop intensity profile was measured on CCD_1. With a PFM acting in a reflective capacity, the FTB was directed to the right half of the SLM screen, and the resulting beam was measured on CCD_2 after reflection off a FM.
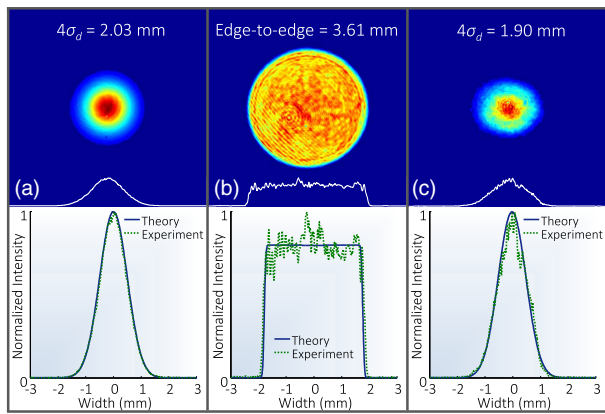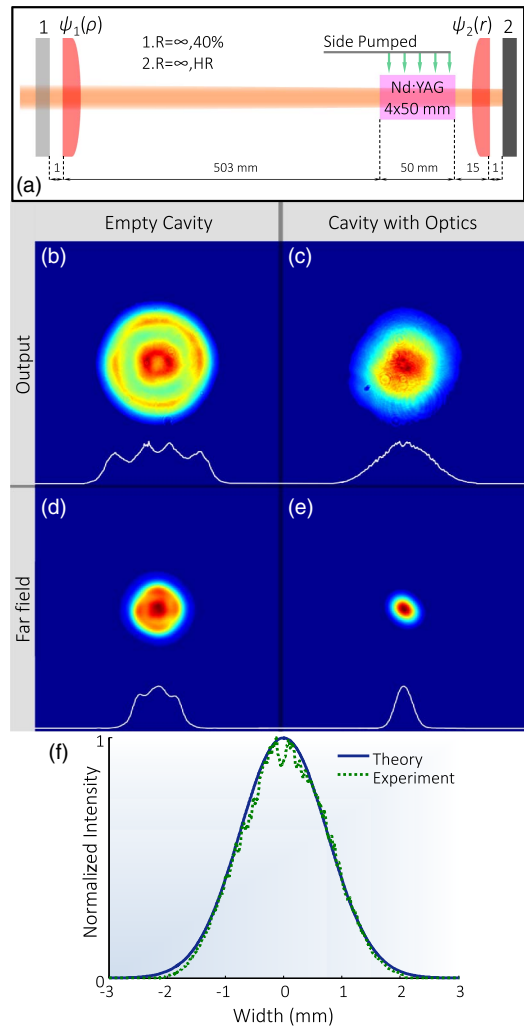
Fig. 5. External optical testing of a single round trip was executed by propagating a collimated (a) Gaussian beam of $w_0 = 1$ mm onto an appropriate phase pattern for transformation to an FTB of width $w_{FTB} = 1.8$ mm. The output resulted in a well-defined (b) FTB of edge-to-edge diameter of 3.61 mm (measured $w_{FTB} = 1.81$ mm). The FTB was directed onto the second element and was transformed to a (c) Gaussian beam (measured $w_0 = 0.95$ mm). The profiles below the 2D beam images demonstrate high overlap between the expected intensities and the experimentally measured intensities.
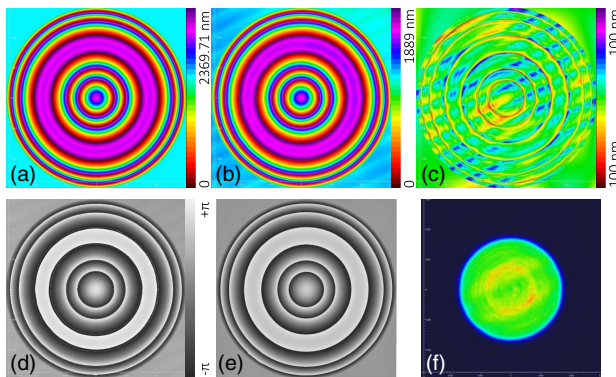
Fig. 6. (a) Laser cavity with the inclusion of the beam transformation elements was compared to an empty cavity. Near-field outputs from the two cavities show (b) multimode operation for the empty cavity and (c) Gaussian-like operation for the custom cavity. The profiles in the Fourier plane of the OC likewise confirm this property, with the empty cavity shown in (d) and the custom cavity in (e). (f) Experimental and theoretical profiles of the output mode from the designed cavity.


Fig. 7. Optics were manufactured using gray-scale lithography with an AZ4562 Photoresist. The manufacturer characterized the components where (a) the target height profile corresponds to our design. (b) The measured height profile using a Zygo interferometer illustrates a maximum height of 1889 nm and is scaled by a factor of about 1.3 due to the etching process and arrives at 2370 nm. This corresponds to an excellent agreement with the target profile. (c) The surface deviation is computed between the target profile and the measured profile. Here the RMS height deviation is minimal and is calculated to be 20 nm. (d) The phase change of the element is calculated and compares exceedingly well to that measured by (e) white-light interferometry. (f) The performance of the measured profile is simulated by modulating a Gaussian beam with this phase. The resulting beam intensity is a uniform flattop.

This was to ensure minimal diffraction effects, with beam widths much smaller than the cavity aperture sizes, which came at the expense of energy extraction (see later discussion). With these parameters, the phase profiles of the two elements under these specifications were computed numerically from Eqs. (3) and (5) and were used in the manufacturing of physical phase-only elements.

The optical elements were 7 mm diameter components, housed in a 25.4 mm diameter holder, which were manufactured from a fused-silica substrate and antireflection-coated for the design wavelength of 1064 nm. The elements were manufactured via gray-scale lithography, where each element was fabricated with an AZ4562 Photoresist. As an example of the characterization

measurements performed by the manufacturer on the optics, we consider the target phase profile of $\psi_1(\rho)$, as shown in Fig. 7(a). Here the target height profile corresponds to a maximum of 2369.71 nm due to the refractive index of the fused-silica ($n = 1.449$) at the design wavelength. The corresponding Zygo interferometric image of the phase of the element [see Fig. 7(b)] illustrates a maximum height profile of 1889 nm. This is the target height in the manufacturing process, as the scaling due to the etching process increases the height by a factor of about 1.3. This corresponds to an actual height on the order of 2370 nm, which is in excellent agreement with the target height.

The surface deviation was also computed by subtracting the target height from the measured height, and the RMS height deviation was determined to be 20 nm, as illustrated in Fig. 7(c). This is an excellent result on the quality of the element, as a 1% wavefront transmission error corresponds to a height deviation of 9 nm, which is roughly 3 orders of magnitude smaller than the spatial resolution of our SLM. Furthermore, the phase change of the measured element was computed, as shown in Fig. 7(d), and compares exceedingly well with the surface profile as measured with white-light interferometry in Fig. 7(e). Finally, the modulation of the designed Gaussian beam was simulated through the measured profile and resulted in a uniform flattop, as shown in Fig. 7(e).

The key point of comparison to the resonator as presented in Fig. 6(a) was an optical resonator of the same cavity length and output mirrors, but without the inclusion of the phase-only optical elements. We refer to this as the "empty cavity." The output of the empty cavity at 20 pps is illustrated in Fig. 6(b) and had a measured second-moment beam diameter of $4\sigma = 3.45$ mm. It is clear from the intensity cross sections that the output is not single mode, and this is further verified by sampling the intensity of the output in the Fourier plane of the OC, as shown in Fig. 6(d). The measurement at the Fourier plane was achieved by propagating the output through a convergent lens and sampling the intensity at the focal plane of the lens, thus emulating propagation to the far field. The lens was positioned at a distance larger than its focal length away from the OC. With the insertion of the optical elements in the cavity, the output at 20 pps is very close to Gaussian in shape, as illustrated in Fig. 6(c) with a measured second-moment beam diameter of $4\sigma = 2.95$ mm, which is in excellent agreement with the design parameter of 3 mm. The Gaussian shaped output was validated as a low-order mode by retaining its shape in the far field, as shown in Fig. 6(e). A comparison of the experimentally measured and theoretically designed output profile is shown in Fig. 6(f). The output of the empty cavity and the cavity with the optics inserted were analyzed in terms of the beam quality (M^2) and output energy, which were used to determine the brightness at the output. An ISO-compliant method [41] was used to determine the M^2, where experimentally, the output of the cavity was transmitted through a convergent lens. The resulting 4σ beam diameter at the focus position along the propagation axis ($z = 0$ mm corresponds to the plane of the lens) was measured with a CCD camera. The camera was then shifted along the propagation axis until the beam size had increased by $\sqrt{2}$ from that at the focus position. The distance between these two measurements was then used to compute the Rayleigh range (z_R). With this, 28 more measurements were captured, seven on either side of the waist within the Rayleigh range and seven on either side of the waist beyond the Rayleigh range. In obtaining the M^2, the squares of the corresponding beam radii were plotted against their respective z positions from the lens. The data points were fitted with a second-order polynomial (of the form $Y = Ax^2 + Bx + C$), and the coefficients were extracted and applied to the following expression: $M^2 = (\pi/\lambda)(AC - B^2/4)^{1/2}$ to obtain the M^2. This resulted in $M^2 = 4.03$ for the empty cavity. With the optics inserted in the cavity, the measured M^2 improved dramatically as compared to the empty cavity and resulted in $M^2 = 1.55$, confirming that the output was a lower divergence Gaussian-like beam.

The measured output energy and beam quality of the cavities were used to determine the optical brightness from Eq. (1).

(a)

(b)
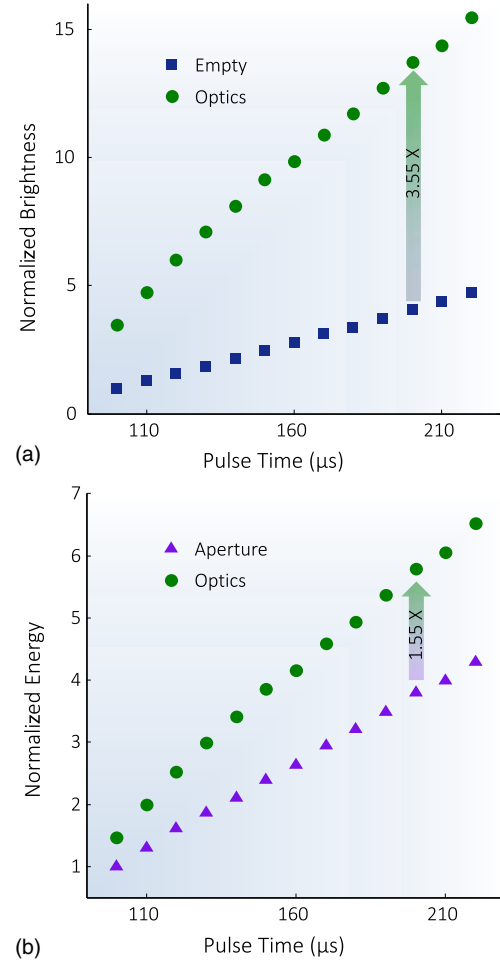
Fig. 8. (a) Measured brightness enhancement for the designed cavity with the optics as compared to the open cavity. The slope difference equates to an approximate enhancement factor of 350%. (b) Measured energy extraction enhancement for the designed cavity with the optics as compared to a cavity apertured to the same size. The slope difference equates to an approximate enhancement factor of ~55%.

Without any adjustment for gain volume and comparing the performances directly, we find an increase in laser brightness by over 350%, as shown in Fig. 8(a). The increase in optical brightness illustrates a marked improvement on the empty cavity.

4. DISCUSSION

The brightness enhancement can be expressed very simply as

$$\eta = \frac{B_{\mathrm{new}}}{B_0} = \epsilon \left(\frac{M_0^2}{M_{\mathrm{new}}^2} \right)^2, \qquad (7)$$

where "new" refers to measured parameters of the cavity with the optics, the subscript 0 refers to the original reference cavity, and $\epsilon = P_{\mathrm{new}}/P_0$ is the ratio of the power extraction from the two cavities. Because the gain volume of the two cavities was not the same, their extraction was markedly different. The small FTB meant a designed gain volume of only half that of the empty cavity, i.e., $\epsilon = 0.5$. Even with this designed energy loss, the measured enhancement was $\eta = 3.5$, a notable achievement. The measured power extraction was $\epsilon = 0.475$ with the additional ~2.5% loss attributed to losses imposed by the optical elements,

length optimization, and alignment. This confirms the theoretically expected $\epsilon \approx 1$ if the gain media had the same size (since the multimode beam from the empty cavity also has a high overlap with the gain medium), giving a predicted $\eta \approx 7$ for our design.

To compare two cavities of the same gain size, we inserted an aperture into the empty cavity to reduce the gain volume to that of the diffractive optical element (DOE) cavity. The result in this case was a new $\epsilon = 1.55$, shown in Fig. 8(b). This highlights some interesting points: First, that as indicated before, the FTB is very efficient at extracting energy because of the overlap with the gain. Here we see that it outperforms a conventional cavity on energy extraction by about ∼55% because the apertured cavity no longer operates on a multimode beam and so does not have a very good gain-mode overlap. In this case, the enhancement is smaller, $\eta = 1.1$, since the apertured cavity now has a better mode quality but less energy. This test essentially compares two Gaussian mode cavities and reveals that the mode-morphing cavity allows the same beam quality but with better energy extraction. When the aperture in the conventional cavity was opened, the mode quality deteriorated so that although the energy increased, the brightness decreased. This is the status quo for resonators: Opening apertures allows more modes to oscillate so that the energy extracted is higher, but the mode quality suffers: mode quality and energy extraction are coupled, since the mode is the same profile everywhere in the cavity. The salient point here is that the route to high brightness involves maximizing both energy extraction and mode quality simultaneously, and our approach demonstrates that this is now possible: We maintain the same output profile (Gaussian) by design, and independently design the profile needed to extract energy efficiently, which is possible because we have the freedom to change the mode shape inside the cavity.

Although our design offers brightness *enhancement*, the maximum brightness attainable will still be limited by other effects, such as thermal lensing, thermal aberrations, stress-induced perturbations, and so on—factors usually associated with high thermal loads in the gain medium. Our approach requires a uniformly illuminated gain, and so comparison to any similarly pumped laser will imply similar aberrations: the thermal gradient in both systems will be identical and will result in a degradation of both cavity outputs. However, in our cavity, it is a Gaussian beam that degrades rather than a multimode beam, so the improvement in initial mode quality still implies a substantial benefit in brightness enhancement. When compared to an empty cavity that is engineered to select a Gaussian mode, the required Gaussian pump (for efficient energy extraction) has some deleterious effects: A Gaussian pump has a much larger peak intensity than a flattop pump (assuming the same energy) due to the Gaussian shape and small size to avoid diffraction effects. Our simulations indicate that this will result in a much larger thermal gradient than for our flattop pumped cavity. Thus, while both cavities will output a Gaussian beam, our cavity will output one that is less aberrated, suggesting an even better enhancement in comparative brightness. Furthermore, the thermal aberration may be measured or theoretically determined and incorporated into the design of our elements so as to negate its effect at a fixed pump power.

The theoretical limit to the enhancement that one might see, assuming that the overlap of the gain is already optimized, is $\eta \to (M_0^2)^2$, that is, it is entirely determined by how poor the original cavity is in terms of mode quality. For our cavity, this value is approximately 7×. In particular, this concept may be revolutionary for slab laser designs. The M_0^2 in the long axis can be well over 100. Applying this principle to such a cavity would require a 1D rather than 2D beam-shaping solution and would have a predicted brightness enhancement of several orders of magnitude: high brightness Gaussian beams from slab lasers.

5. CONCLUSION

We have demonstrated a high-brightness solid-state laser that optimizes both energy extraction and beam quality, two parameters that are usually anticorrelated, i.e., increasing one tends to decrease the other. We achieve this by introducing a new design paradigm whereby the laser mode inside the cavity changes continuously from one desired shape to another. By specifying an FTB at the gain end and a Gaussian beam at the OC end, the output from the cavity has optimized energy, but in a low divergence Gaussian beam. We demonstrated the concept on an off-the-shelf commercial laser that was not adjusted in any way other than to insert two custom-designed phase-only optical elements into the cavity. The effect of doing this was to dramatically enhance the measured performance in terms of output brightness by 350%, possible through the concept of mode metamorphosis inside a laser cavity.

We point out that this concept is not restricted to these two particular intensity profiles and may be suitably adapted for alternative geometries, e.g., rectangular beams for a slab configuration or annular beams for annular gain. Our demonstration therefore serves as a general approach to optimizing laser brightness from laser cavities.

REFERENCES

1. A. E. Siegman, "New developments in laser resonators," Proc. SPIE **1224**, 2–14 (1990).
2. C. X. Yu, S. J. Augst, S. M. Redmond, K. C. Goldizen, D. V. Murphy, A. Sanchez, and T. Y. Fan, "Coherent combining of a 4 kW, eight-element fiber amplifier array," Opt. Lett. **36**, 2686–2688 (2011).
3. L. P. Ramirez, M. Hanna, G. Bouwmans, H. El Hamzaoui, M. Bouazaoui, D. Labat, K. Delplace, J. Pouysegur, F. Guichard, P. Rigaud, V. Kermène, A. Desfarges-Berthelemot, A. Barthélémy, F. Prévost, L. Lombard, Y. Zaouter, F. Druon, and P. Georges, "Coherent beam combining with an ultrafast multicore Yb-doped fiber amplifier," Opt. Express **23**, 5406–5416 (2015).
4. T. Y. Fan, "Laser beam combining for high-power, high-radiance sources," IEEE J. Sel. Top. Quantum Electron. **11**, 567–577 (2005).
5. H. Injeyan and G. Goodno, *High Power Laser Handbook* (McGraw-Hill, 2011), Chap. 19.
6. P. Sprangle, B. Hafizi, A. Ting, and R. Fischer, "High-power lasers for directed-energy applications," Appl. Opt. **54**, F201–F209 (2015).
7. S. M. Redmond, K. J. Creedon, J. E. Kansky, S. J. Augst, L. J. Missaggia, M. K. Connors, R. K. Huang, B. Chann, T. Y. Fan, G. W. Turner, and A. Sanchez-Rubio, "Active coherent beam combining of diode lasers," Opt. Lett. **36**, 999–1001 (2011).
8. J. Montoya, S. J. Augst, K. Creedon, J. Kansky, T. Y. Fan, and A. Sanchez-Rubio, "External cavity beam combining of 21 semiconductor lasers using SPGD," Appl. Opt. **51**, 1724–1728 (2012).

9. K. J. Creedon, S. M. Redmond, G. M. Smith, L. J. Missaggia, M. K. Connors, J. E. Kansky, T. Y. Fan, G. W. Turner, and A. Sanchez-Rubio, "High efficiency coherent beam combining of semiconductor optical amplifiers," Opt. Lett. **37**, 5006–5008 (2012).

10. A. E. Siegman, "Laser beams and resonators: the 1960s," IEEE J. Sel. Top. Quantum Electron. **6**, 1380–1388 (2000).

11. A. E. Siegman, "Laser beams and resonators: beyond the 1960s," IEEE J. Sel. Top. Quantum Electron. **6**, 1389–1399 (2000).

12. N. Hodgson and H. Weber, *Laser Resonators and Beam Propagation* (Springer, 2005), p. 476.

13. P. A. Bélanger and C. Paré, "Optical resonators using graded-phase mirrors," Opt. Lett. **16**, 1057–1059 (1991).

14. C. Paré, L. Gagnon, and P. A. Bélanger, "Aspherical laser resonators: an analogy with quantum mechanics," Phys. Rev. A **46**, 4150–4160 (1992).

15. C. Paré and P. A. Bélanger, "Custom laser resonators using graded-phase mirrors," IEEE J. Quantum Electron. **28**, 355–362 (1992).

16. I. A. Litvin and A. Forbes, "Intra-cavity flat-top beam generation," Opt. Express **17**, 15891–15903 (2009).

17. I. A. Litvin and A. Forbes, "Gaussian mode selection with intracavity diffractive optics," Opt. Lett. **34**, 2991–2993 (2009).

18. M. Kuznetsov, M. Stern, and J. Copetta, "Single transverse mode optical resonators," Opt. Express **13**, 171–181 (2005).

19. B. Tiffany and J. Leger, "Losses of bound and unbound custom resonator modes," Opt. Express **15**, 13463–13475 (2007).

20. J. R. Leger, D. Chen, and Z. Wang, "Diffractive optical element for mode shaping of a Nd:YAG laser," Opt. Lett. **19**, 108–110 (1994).

21. P. A. Bélanger, R. L. Lachance, and C. Paré, "Super-Gaussian output from a CO_2 laser by using a graded-phase mirror resonator," Opt. Lett. **17**, 739–741 (1992).

22. M. Gerber and T. Graf, "Generation of super-Gaussian modes in Nd:YAG lasers with a graded-phase mirror," IEEE J. Quantum Electron. **40**, 741–746 (2004).

23. A. J. Caley, M. J. Thomson, J. Liu, A. J. Waddie, and M. R. Taghizadeh, "Diffractive optical elements for high gain lasers with arbitrary output beam profiles," Opt. Express **15**, 10699–10704 (2007).

24. T. Y. Cherezova, L. N. Kaptsov, and A. V. Kudryashov, "Cw industrial rod YAG:Nd³⁺ laser with an intracavity active bimorph mirror," Appl. Opt. **35**, 2554–2561 (1996).

25. T. Y. Cherezova, S. S. Chesnokov, L. N. Kaptsov, and A. V. Kudryashov, "Super-Gaussian laser intensity output formation by means of adaptive optics," Opt. Commun. **155**, 99–106 (1998).

26. T. Y. Cherezova, S. S. Chesnokov, L. N. Kaptsov, V. V. Samarkin, and A. V. Kudryashov, "Active laser resonator performance: formation of a specified intensity output," Appl. Opt. **40**, 6026–6033 (2001).

27. W. Lubeigt, G. Valentine, J. Girkin, E. Bente, and D. Burns, "Active transverse mode control and optimization of an all-solid-state laser using an intracavity adaptive-optic mirror," Opt. Express **10**, 550–555 (2002).

28. W. Lubeigt, M. Griffith, L. Laycock, and D. Burns, "Reduction of the time-to-full-brightness in solid-state lasers using intra-cavity adaptive optics," Opt. Express **17**, 12057–12069 (2009).

29. M. Gerber, T. Graf, and A. Kudryashov, "Generation of custom modes in a Nd:YAG laser with a semipassive bimorph adaptive mirror," Appl. Phys. B **83**, 43–50 (2006).

30. S. Ngcobo, K. Ait-Ameur, I. Litvin, A. Hasnaoui, and A. Forbes, "Tuneable Gaussian to flat-top resonator by amplitude beam shaping," Opt. Express **21**, 21113–21118 (2013).

31. I. A. Litvin, G. King, and H. Strauss, "Beam shaping laser with controllable gain," Appl. Phys. B **123**, 174 (2017).

32. R. Sundar, K. Ranganathan, and S. Oak, "Generation of flattened Gaussian beam profiles in a Nd:YAG laser with a Gaussian mirror resonator," Appl. Opt. **47**, 147–152 (2008).

33. D. Naidoo, A. Harfouche, M. Fromager, K. Ait-Ameur, and A. Forbes, "Emission of a propagation invariant flat-top beam from a microchip laser," J. Luminesc. **170**, 750–754 (2016).

34. R. L. Byer, "Diode pumped solid state lasers," in *Conference on Lasers and Electro-Optics/Pacific Rim* (Optical Society of America, 2009).

35. T. Y. Fan and R. L. Byer, "Diode laser-pumped solid-state lasers," IEEE J. Quantum Electron. **24**, 895–912 (1988).

36. W. Koechner, *Solid-State Laser Engineering* (Springer, 2006), p. 193.

37. A. Siegman, *Lasers* (University Science Books, 1986), p. 706.

38. J. R. Leger, D. Chen, and K. Dai, "High modal discrimination in a Nd:YAG laser resonator with internal phase gratings," Opt. Lett. **19**, 1976–1978 (1994).

39. L. A. Romero and F. M. Dickey, "Lossless laser beam shaping," J. Opt. Soc. Am. A **13**, 751–760 (1996).

40. N. Barré, M. Romanelli, and M. Brunel, "Role of cavity degeneracy for high-order mode excitation in end-pumped solid-state lasers," Opt. Lett. **39**, 1022–1025 (2014).

41. ISO, "Test methods for laser beam widths, divergence angles and beam propagation ratios. Part 1: stigmatic and simple astigmatic beams," ISO 11146-1:2005 (2005).